Journal Pre-proofs

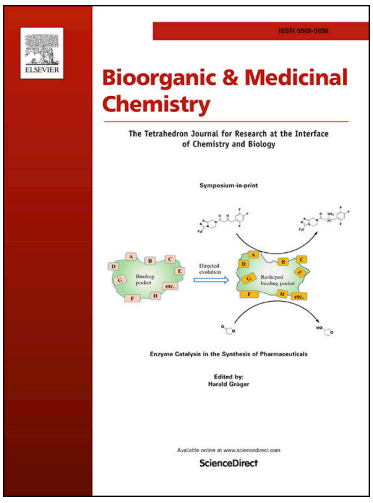

Ferulic Acid Amide Derivatives with Varying Inhibition of Amyloid-β Oligomerization and Fibrillization

Igri Kolaj, Yanfei Wang, Kailin Ye, Autumn Meek, S. Imindu Liyanage, Clarissa Santos, Donald F. Weaver

PII: S0968-0896(21)00255-8
DOI: https://doi.org/10.1016/j.bmc.2021.116247
Reference: BMC 116247

To appear in: *Bioorganic & Medicinal Chemistry*

Received Date: 25 February 2021
Revised Date: 19 May 2021
Accepted Date: 28 May 2021

Please cite this article as: I. Kolaj, Y. Wang, K. Ye, A. Meek, S. Imindu Liyanage, C. Santos, D.F. Weaver, Ferulic Acid Amide Derivatives with Varying Inhibition of Amyloid-β Oligomerization and Fibrillization, *Bioorganic & Medicinal Chemistry* (2021), doi: https://doi.org/10.1016/j.bmc.2021.116247

Ferulic Acid Amide Derivatives with Varying Inhibition of Amyloid-β Oligomerization and Fibrillization

Igri Kolaj[a,b], Yanfei Wang[b], Kailin Ye[b,c], Autumn Meek[b], S. Imindu Liyanage[b], Clarissa Santos[b], Donald F. Weaver[a,b,c,*]

[a] Department of Chemistry, University of Toronto
80 St. George Street, Toronto, ON M5S 3H6, Canada

[b] Krembil Research Institute, University Health Network,
Krembil Discovery Tower, 60 Leonard Avenue, 4KD477, Toronto, ON M5T 0S7, Canada

[c] Department of Pharmaceutical Chemistry, University of Toronto
144 College Street, Toronto, ON M5S 3M2, Canada

Corresponding author:
Donald F. Weaver,
donald.weaver@utoronto.ca
60 Leonard Avenue, 4KD477, Toronto, ON M5T 0S7, Canada

Other authors:
Igri Kolaj: igri.kolaj@gmail.com; Yanfei Wang: yanfei.trv@gmail.com; Kailin Ye: kailin.ye@mail.utoronto.ca; Autumn Meek: autumn.meek@gmail.com; S. Imindu Liyanage: imindu.liyanage@mail.utoronto.ca; Clarissa Santos: clarissa.santos@uhnresearch.ca

Declarations of interest: None.

Funding: This research did not receive any specific grant from funding agencies in the public, commercial, or not-for-profit sectors.

Key Words: Alzheimer's disease; Aβ oligomerization; Aβ fibrillization; ferulic acid; curcumin; amide derivatives.

Abstract

Alzheimer's disease (AD) is a progressive neurodegenerative disorder characterized by the misfolding, oligomerization and fibrillization of amyloid-β (Aβ). Evidence suggests that the mechanisms underpinning Aβ oligomerization and subsequent fibrillization are distinct, and may therefore require equally distinct therapeutic approaches. Prior studies have suggested that amide derivatives of ferulic acid, a natural polyphenol, may combat multiple AD pathologies, though its impact on Aβ aggregation is controversial. We designed and synthesized a systematic library of amide derivatives of ferulic acid and evaluated their anti-oligomeric and anti-fibrillary capacities independently. Azetidine tethered, triphenyl derivatives were the most potent anti-oligomeric agents (compound **2i**: IC_{50} = 1.8μM ± 0.73μM); notably these were only modest anti-fibrillary agents (20.57% inhibition of fibrillization), and exemplify the poor correlation between anti-oligomeric/fibrillary activities. These data were subsequently codified in an *in silico* QSAR model, which yielded a strong predictive model of anti-Aβ oligomeric activity (κ = 0.919 for test set; κ = 0.737 for validation set).

Word Count: 156

Graphical Abstract

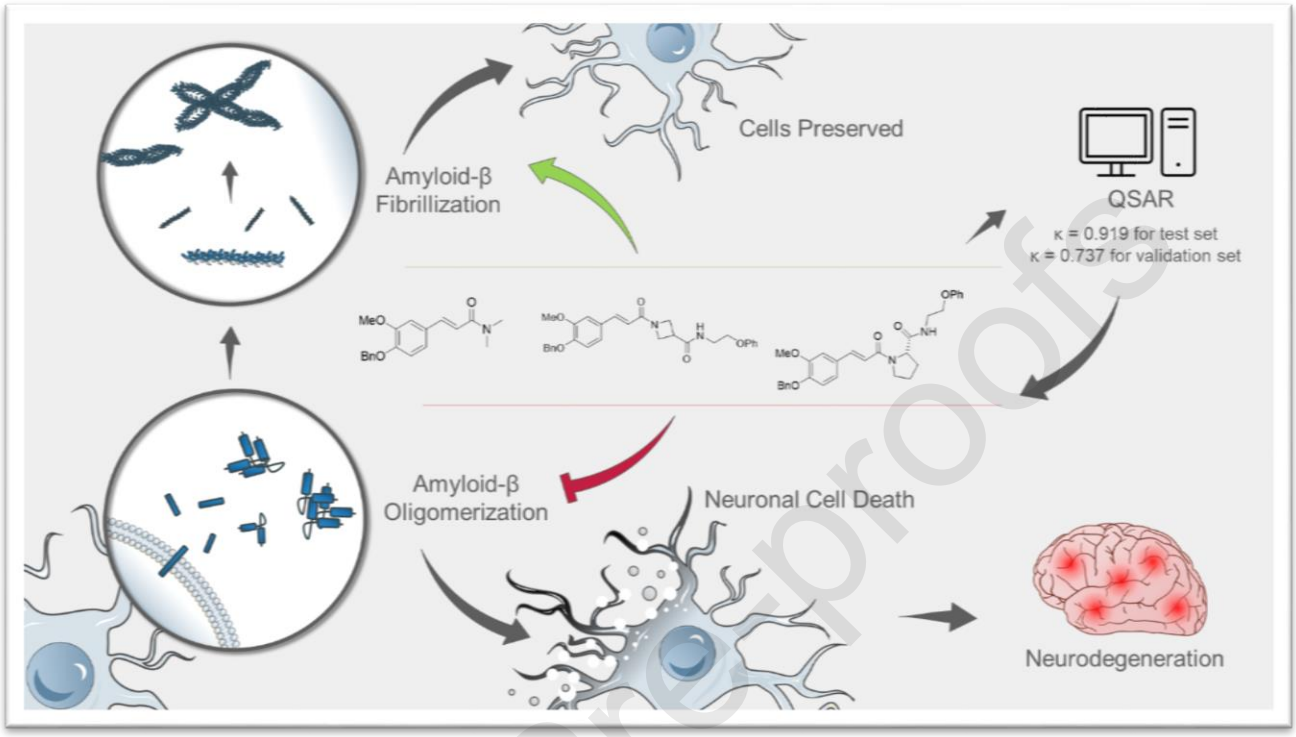

1. Introduction

Aggregation of misfolded proteins is central to the leading mechanistic hypotheses for major neurodegenerative disorders, including Parkinson's disease, prion encephalopathies and Alzheimer's disease (AD). In AD, these aggregates induce neuroinflammation, neuronal death and cerebral atrophy – manifesting as progressive declines in cognition, memory and executive function.[1] Despite exhaustive study, neither a definitive therapy nor a clear therapeutic target have been discerned; rather an array of diverse and interconnected pathologies, ranging from innate immunity to mitochondrial dysfunction, has been suggested as causative.[1] However, the misfolding and aggregation of neural proteins, be it symptomatic or etiological, remain the best studied AD pathology and a continued focus of major therapeutic strategies.

AD is characterized by two dominant protein pathologies: the accumulation of neurofibrillary tangles composed of hyperphosphorylated filaments of protein tau, and the formation of extracellular amyloid plaques, composed of amyloid-β (Aβ) peptides.[2, 3] Previously, Aβ aggregation was thought to be the definitive step in the onset and progression of AD.[3-7] This *amyloid hypothesis* purported that soluble oligomeric species of Aβ triggered a cascade of downstream events including neuronal damage, immune activation, tau phosphorylation, microglial activation and cytokine/chemokine release, that ultimately culminate in neuronal death and the clinical manifestations of AD.[8] Though the etiology has since proven more nuanced, with Aβ likely acting in complex synergies to yield the observed changes, it remains the best studied target in AD. Agents interfering with the oligomerization and fibrillization (collectively referred to as "aggregation") of Aβ have therefore been among the most intensely examined. To date, numerous small molecules, natural and synthetic, have been proposed with

some activity against the aggregation of Aβ. Among these, natural polyphenols, derived from plants have repeatedly shown promise.[9-11]

In early work, the polyphenol curcumin, demonstrated notable anti-amyloidogenic activity as well as antioxidative and anti-inflammatory properties *in vitro*,[12] *in vivo*,[13] and *in silico*.[14,15] In plants, it is formed from the dimerization of ferulic acid, itself a potent antioxidant,[15-18] and a potential multifunctional agent against AD.[19-22] Recent studies have shown that administration of ferulic acid, either alone or in combination, can rescue neurodegeneration and cognitive decline in AD,[23] as well as other disease indications.[24] Prior derivatives of ferulic acid have also conferred multifaceted protective associations *in vitro*,[25] though their capacity as anti-aggregative agents is disputed. Further, clinical trials have yet to show a significant effect on cognition or AD progression, likely attributable to inadequate pharmacokinetic properties and blood-brain barrier (BBB) permeability. Curcumin may also readily undergo oxidative degradation within the aqueous physiology of the body, further complicating its utility as a therapeutic.

More recently recognized biophysical discrepancies between the oligomerization and fibrillization of Aβ may also be partly culpable.[26-28] Though formerly considered synonymous processes, data now suggest that the mechanisms underpinning the aggregation of Aβ into small oligomeric species, and the subsequent aggregation into larger fibrils are distinct. Of particular relevance to therapeutic strategies was the observation that oligomers appear highly neurotoxic, while fibrils and plaques are likely benign, and may be a protective strategy to sequester harmful oligomers. Therefore, agents which impede fibrillization, without targeting oligomerization, may leave highly neurotoxic oligomers unaffected, and may deprive the brain of the ability to sequester Aβ. Evidence also suggests that Aβ may be able to circumvent the inhibition of

oligomerization by forming disordered species that can nucleate and aggregate into larger plaques.[28, 29]

To date, studies have relied largely on the inhibition of easily visualized fibrillization (or protofibrils), rather than oligomerization to determine the efficacy of compounds. Yet the differing aggregation of oligomers and fibrils suggest that the functional moieties conferring anti-oligomeric activity may be distinct from those required to prevent fibrillization. The failure to make a clear distinction, and directly target the inhibition of neurotoxic oligomers, may partly explain the failure of amyloid-based therapeutic strategies thus far.

Herein, we systematically evaluate the anti-amyloidogenic activities (both anti-fibrillary and anti-oligomeric) of amide derivatives of ferulic acid. Plant derived amides are highly active within biological systems. Replacement of carboxylic acids with amides is also known to improve BBB penetration, while preserving many of the desirable molecular characteristics. Moreover, amides are amenable to chemical modification, and are therefore a reasonable drug-design platform. We further observed that amide substitution of ferulic acid's carboxylate moiety yielded a 10-fold increase in anti-amyloid activity (Table 1). We assayed these novel amide derivatives specifically as anti-oligomeric agents against Aβ; relevant compounds were further assayed for their anti-fibrillary functionality. These results were used in the construction of a binary QSAR model, which proved capable of accurately predicting the activity of novel compounds.

2. Results and Discussion

2.1 Synthesis of Ferulic Acid Derivatives

A diverse library of amide-based ferulic acid derivatives was constructed. These derivatives were developed to explore differences in electronic, geometric and physicochemical properties in influencing the ferulate analogues to inhibit Aβ oligomer and/or fibril formation. Collectively, this library systematically explores three structural "faces" of ferulic acid: (i) the carboxylic acid moiety – converted to an amide, (ii) the hydroxyl group on the phenol ring, and (iii) the rigid, planar backbone between the carboxylic acid (substituted amide) and aromatic ring.

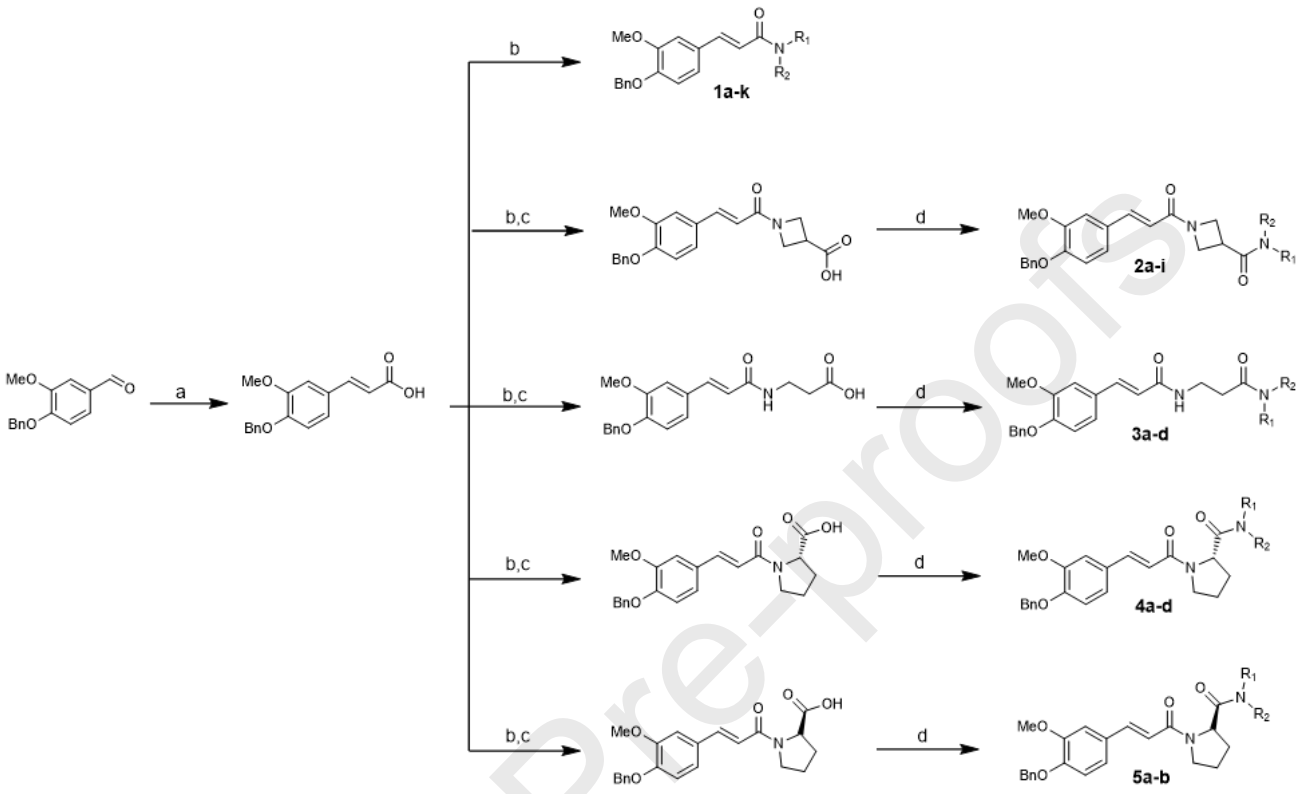

Scheme 1. Synthesis of Ferulic Acid Analogs
Reagents and conditions: (a) malonic acid, pyridine, 110˚C, 14 h; (b), HATU, i-Pr2NEt, amine, DMF, room temperature (rt), 16− 24 h; (c) LiOH, THF/H_2O, 16-24 h; (d) HATU, i-Pr2NEt, amine, DMF, 35˚C or 50˚C, 16− 24 h.

2.2 Inhibition of Aβ Oligomerization

To assess anti-oligomeric activity, an enzyme-linked immunosorbent assay (ELISA), previously described by Levine et al.,[30] was adapted for this study. Unlike assays of fibrillization, this method directly quantifies the abundance of oligomers (relative to monomers) with high sensitivity and minimal interference. Specifically, bio-tinylated $A\beta_{42}$ (bio-$A\beta_{42}$), was allowed to oligomerize in the presence of compounds in a decreasing concentration gradient, and the resulting oligomers were visualized employing a NeutrAvidin/streptavidin protocol. If compounds were functional, a sigmoidal curve of inhibition would be formed and used to estimate the concentration required to inhibit 50% oligomerization (IC_{50}). Compounds with no discernable difference in the abundance of oligomers, or those which did not exhibit any pattern of inhibition were deemed to have no activity (N.A.).

2.2.1 Carboxylic Acid Derivatives

In initial testing, the dimer of ferulic acid (curcumin; compound **0a**) proved substantially more effective against Aβ oligomerization (IC_{50} = 3.38μM ± 0.11μM) than monomeric ferulic acid (compound **0**; IC_{50} = 226.23μM ± 22.26μM). This suggests a relatively large area of interaction between Aβ monomers, which may best be targeted with sterically bulky substitutions on the carboxylic acid. In the first screen of derivatives (Table 1), the parent alkyl amide (modified with a benzyl group at the phenyl hydroxide; section 2.5) was substituted with a variety of alkyl, aromatic, halide and cyclic substituents.

Table 1
Calculated IC_{50} against Aβ oligomerization for carboxyl–derivatives of ferulic acid amides

Comp.	Structure	bio-Aβ_{42} IC_{50} (μM)	Comp.	Structure	bio-Aβ_{42} IC_{50} (μM)
	Ferulic Acid			Curcumin	
0	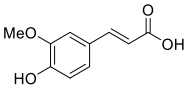	226.23 ± 22.26	**0a**	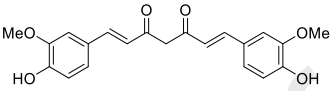	3.85 ± 0.11
1	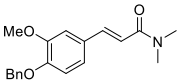	24.60 ± 15.64	**1f**	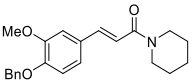	27.94 ± 3.35
1a	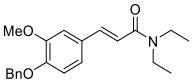	39.27 ± 0.85	**1fa**	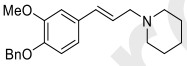	10.64 ± 3.47
1aa	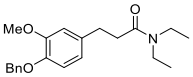	34.93 ± 23.38	**1fb**	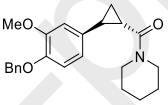	18.65 ± 2.28
1ab	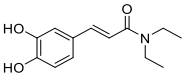	119.16 ± 2.65 μM	**1fc**	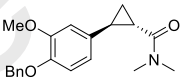	45.78 ± 17.18
1ac	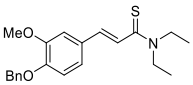	N.A.	**1g**	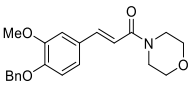	78.07 ± 12.04
1b	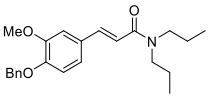	12.38 ± 4.13	**1h**	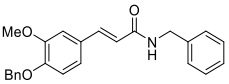	N.A.
1c	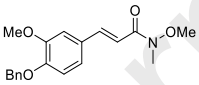	79.87 ± 2.2	**1i**	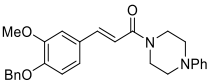	N.A
1d	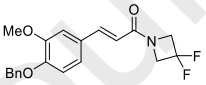	106.82 ± 16.39	**1j**	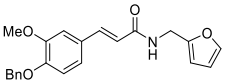	N.A.
1e	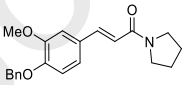	65.09 ± 8.61	**1k**	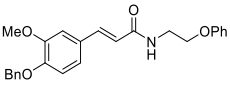	N.A.

N.A. denotes no discernable activity; uncertainty denotes standard deviation. All compounds were assessed in at least three independent samples, with a minimum of three measurements.

A simple alkyl side-chain, cyclic or acyclic, proved most effective against oligomerization (compounds **1**: IC_{50} = 24.60μM ± 15.64μM; **1b**: IC_{50} = 12.38μM ± 22.26μM; and **1f**: IC_{50} = 27.94μM ± 22.26μM). Polar bonds in the region immediately adjacent to the amide proved highly ineffective – suggesting interactions among hydrophobic residues in this space. The carbonyl group of the amide was also critical; when replaced with a thiocarbonyl, all activity was lost. Since amides and thioamides are isosterically similar, it is possible that hydrogen bonding between the carbonyl and an associated residue facilitates interaction with Aβ. However, when the carbonyl was removed entirely (compound **1f**: IC_{50} = 27.94μM ± 3.35μM vs. **1fa**: IC_{50} = 10.64μM ± 3.47μM) the efficacy of the compound rose. Therefore, polar bonds in this region likely hinder interactions with Aβ, yet the carbonyl oxygen may overcome this via hydrogen bonding.

A subsequent series of compounds (Tables 2-3), built upon this initial carbonyl/alkyl spacer, was designed to mimic curcumin's elongated, π-rich structure (Scheme 1). Longer spans were therefore incorporated to add surface area to the molecules, and thus maximize exposure to the wide amyloidogenic residues between Aβ monomers. (S)- and (R)-proline (Table 2) as well as β-alanine (Table 3) were selected as scaffolds, to match the conformational arrangement of curcumin. Among these, the proline derivatives proved moderately effective, yet were generally weaker inhibitors than the initial shorter amides. The presence of a polar amide group in relative proximity to the ferulic amide may be partly explain the lack of improvement.

Table 2
Calculated IC_{50} against Aβ oligomerization for proline carboxyl–derivatives of ferulic acid amides

Comp.	Structure	bio-Aβ_{42} IC_{50} (μM)	Comp.	Structure	bio-Aβ_{42} IC_{50} (μM)
2a	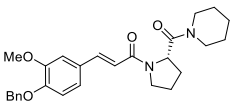	17.08 ± 4.36	**2d**	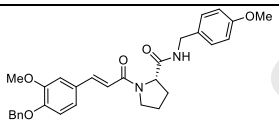	19.24 ± 2.06
2b	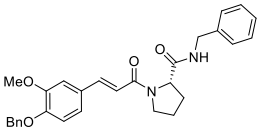	18.72 ± 3.74	**2e**	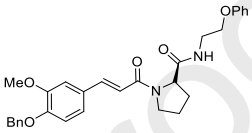	16.83 ± 1.17
2c	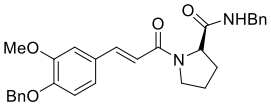	17.75 ± 3.63	**2f**	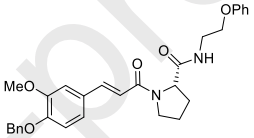	8.59 ± 2.65

Uncertainty denotes standard deviation. All compounds were assessed in at least three independent samples, with a minimum of three measurements.

Table 3
Calculated IC_{50} against Aβ oligomerization for β-alanine carboxyl–derivatives of ferulic acid amides

Comp.	Structure	bio-$A\beta_{42}$ IC_{50} (μM)	Comp.	Structure	bio-$A\beta_{42}$ IC_{50} (μM)
3a	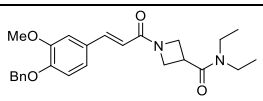	12.78 ± 0.17	**3f**	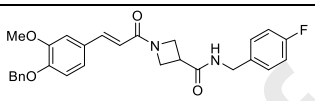	3.65 ± 0.33
3b	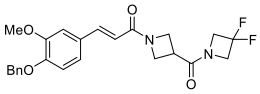	21.83 ± 0.74	**3g**	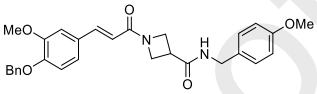	4.78 ± 1.67
3c	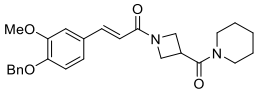	10.55 ± 0.84	**3h**	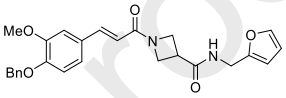	3.61 ± 0.59
3d	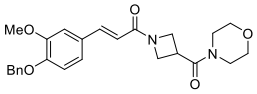	35.67 ± 2.42	**3i**	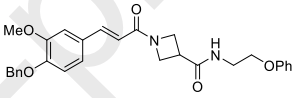	1.80 ± 0.73
3e	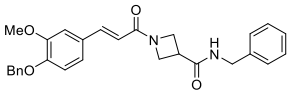	3.13 ± 1.87			
4	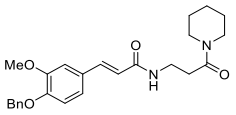	8.17 ± 1.70	**5b**	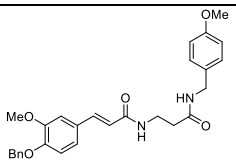	54.21± 2.96
5a	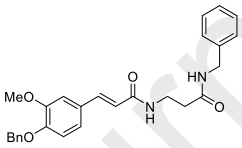	81.56 ± 9.91	**5c**	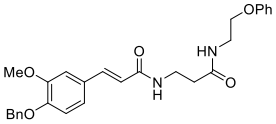	17.91 ± 17.02

N.A. denotes no discernable activity; uncertainty denotes standard deviation. All compounds were assessed in at least three independent samples, with a minimum of three measurements.

Use of a 3-azetidinecarboxylic acid scaffold proved more effective; incorporation of a benzyl-carbamoyl azetidine yielded significant inhibition (compound **3i**; IC_{50} of 1.8μM ± 0.73μM). This triple-phenyl molecule displays a characteristic bent L-shaped conformation (Fig. 1A), which simulates curcumin's spatial arrangement (Fig. 1B), yet is elongated at both ends. The added lateral distance may contribute towards the improved inhibition of Aβ oligomerization. The conformational constraint of the azetidine moiety also appears to be critical. Unlike simple alkyls or higher order rings, the strained azetidine minimizes torsional variation in the backbone, forming a planar link between the ferulic acid and side chain. The success of the azetidine derivatives over the others suggests this conformational restriction facilitates better interaction with Aβ.

Further modification, such as varying the azetidine chain's phenyl ring, did not yield significant changes in function. Even replacement of the phenyl with a furan (compound **3h**) did not alter the IC_{50} substantially – suggesting that π interactions broadly aid the inhibition of Aβ oligomerization in this region. Other major modifications (Table 4), such as incorporation of a tetrazole or oxazole decreased activity, compared to the parent alkyls. Use of an imidazole tether was more effective, achieving an IC_{50} less than 10μM (compounds **11** and **12**), but inhibition was inferior comparable to azetidines. Amongst all tested tethers, the most efficient interaction with Aβ repeatedly occurred in molecules in which the ferulic amide was attached to a 2 carbon alky spacer (ideally rigid), then connected to an additional amide. This polar-nonpolar-polar transition within a localized region appears to facilitate interactions with Aβ.

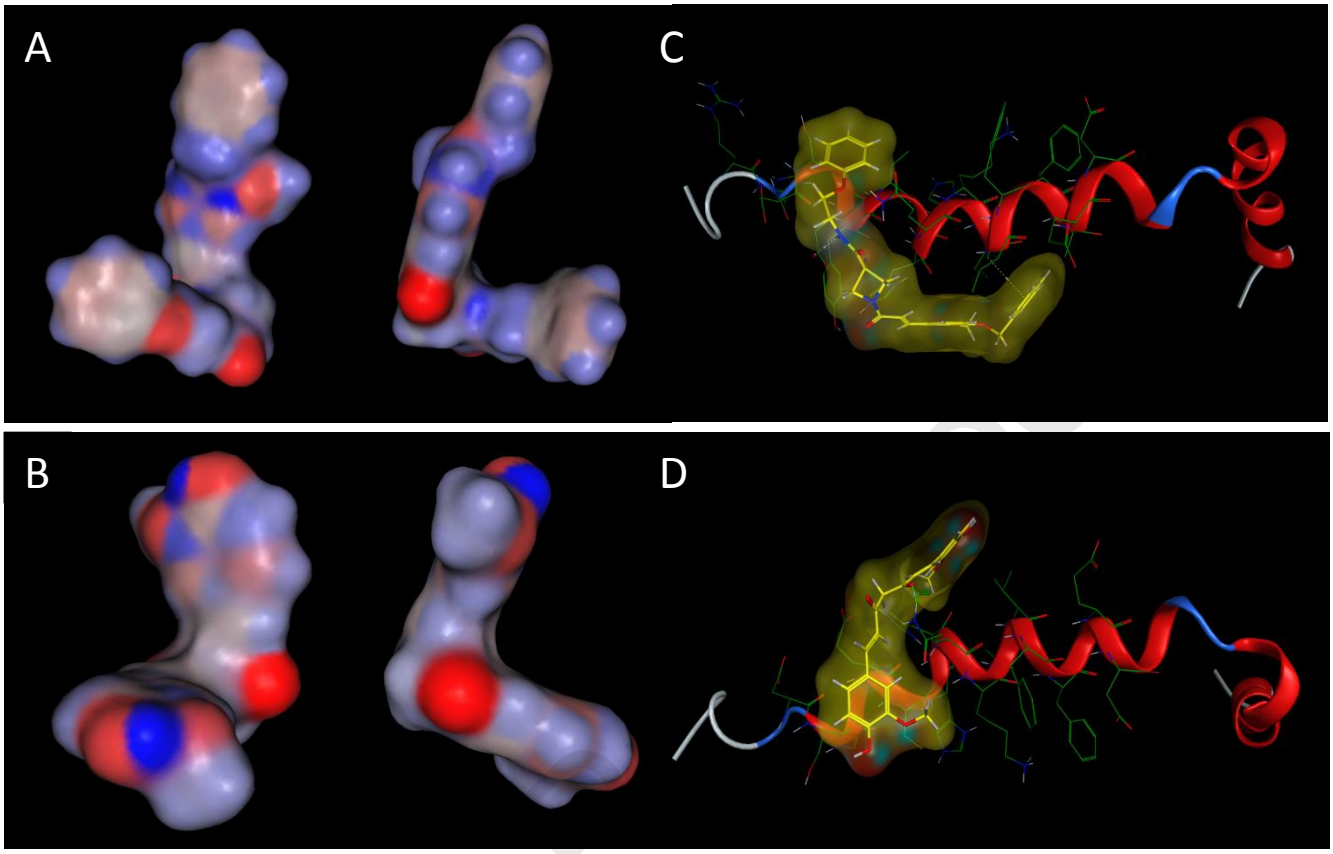

Fig 1. **A & B:** Electron density representation of (A) compound **3i**; phenyl azetidine substituted ferulic acid derivative (IC_{50} = 1.8µM ± 0.73µM); (B) compound **0**; curcumin (IC_{50} = 3.85µM ± 0.11µM). Red denotes electron dense regions, blue denotes electron deficient regions. **C & D:** docking characteristics of (C) compound **3i** and (D) curcumin with Aβ.

Table 4
Calculated IC_{50} against Aβ oligomerization for carboxylate–replaced derivatives of ferulic acid amides

Comp.	Structure	bio-Aβ_{42} IC_{50} (μM)	Comp.	Structure	bio-Aβ_{42} IC_{50} (μM)
6	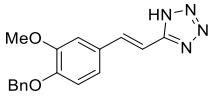	N.A.	**10**	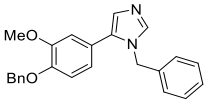	N.A.
7	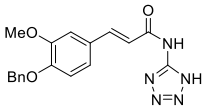	98.46 ± 1.63	**11**	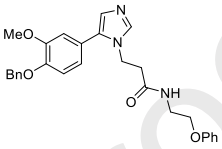	7.76 ± 1.78
8	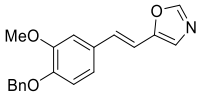	N.A.	**12**	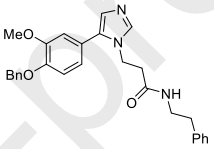	9.91 ± 1.04
9	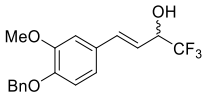	N. A.			

N.A. denotes no discernable activity; uncertainty denotes standard deviation. All compounds were assessed in at least three independent samples, with a minimum of three measurements.

2.2.2 Planar Backbone Derivatives

Unlike the characteristics of the amide, the conformation and saturation of the alkene of ferulic acid is not critical to activity. Saturation and cyclopropanation of the alkene (Table 1: compounds **1aa**, **1fb**,**1fc**) did not yield significant changes in activity - suggesting that the α,β-unsaturated backbone, and the resulting structural conformation, are not crucial for binding to the Aβ peptide. Furthermore, the IC_{50} of compounds **1fc** (45.78μM ± 17.18μM), **1aa** (34.93μM ± 23.38μM) and **1fa** (18.65μM ± 2.28μM), were similar to their parent compounds, **1** (24.6μM ± 15.64μM), **1a** (39.27μM ± 0.85μM) and **1f** (27.94μM ± 3.35 μM) respectively, suggesting that the activity is not due to a false positive caused by nucleophilic addition to the β-position of the Michael acceptor. Ultimately, the replacement of the double bond may be advantageous in the design of therapeutics, as metabolic stability and brain penetrance may be enhanced by the removal a potential Michael acceptor.

2.2.3 Phenyl Substitutions

The phenyl group of ferulic acid was generally not amenable to substitution. Two simple alkyl-amides (with moderate activity) were selected as parent molecules, and substituted with several side chains. In both cases, replacing the hydroxide with a phenyl ether, substantially increased anti-oligomeric activity (Table 5: 13a vs. 13b; 14a vs. 14b). As with the carboxyl-arm, it is likely the added benzene facilitates further π interactions with Aβ, enabling more energetically favorable interactions between the molecule and peptide. However, most modifications thereafter substantially decreased activity. Adding either electron withdrawing (14e) or donating (14d) groups to the phenyl ring eliminated all discernable activity. Likewise,

lengthening the alkyl chain, or modifying the phenyl ring also decreased activity. Introduction of a toluenesulfonyl (tosyl) group was the sole variation associated with a gain in activity (compound **13c**; IC_{50} = 10.64μM ± 3.47μM). It is notable that the tosyl substituent preserves many elements of the general spatial arrangement of the phenyl ether; yet, its susceptibility to nucleophilic attack and other modification renders it impractical as a potential therapeutic agent. The polarity of the sulfate group would also decrease BBB penetrance, and increase the metabolic burden on the drug. This investigation therefore employed the benzylether for all subsequent molecules.

Table 5
Calculated IC_{50} against Aβ oligomerization for hydroxyl–derivatives of ferulic acid amides

Parent molecule	Comp.	Benzyl Substitution	bio-$A\beta_{42}$ IC_{50} (μM)	Comp.	Benzyl Substitution	bio-$A\beta_{42}$ IC_{50} (μM)
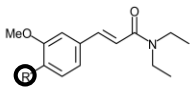	**13a (1a)**	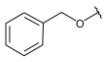	39.27 ± 0.85	**13d**	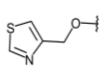	N.A.
	13b		205.46 ± 8.18	**13e**	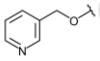	N.A.
	13c	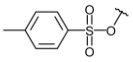	10.64 ± 3.47			
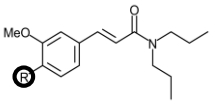	**14a (1b)**	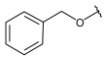	12.38 ± 4.13	**14d**	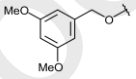	N.A.
	14b		98.79 ± 26.28	**14e**	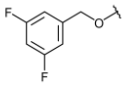	N.A.
	14c		45.31 ± 25.0	**14f**	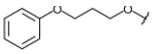	. N.A.

N.A. denotes no discernable activity; uncertainty denotes standard deviation; ® on parent molecule denotes site of substitution. All compounds were assessed in at least three independent samples, with a minimum of three measurements.

2.3 Inhibition of Aβ Fibrillization

Compounds with demonstrated anti-oligomeric activity were tested against fibrillization employing a standard Thioflavin T (ThT) assay. Unlike the direct approach of the oligomer assay, the ThT assay relies on changes in the fluorescence of thioflavin when associated with a large β-pleated sheet structure to quantify the presence of fibrils. Inhibition was calculated as a percent difference in comparison to a non-inhibitory control, averaged after approximately 100 hrs of incubation (Fig. 2, summarized in Table 6). To facilitate aggregation over the experimental time frame, a relatively high concentration of Aβ (20 μM) was employed; compounds were therefore tested at corresponding concentration of 100μM. To mitigate potential anomalies in fluorescence at these concentrations, the relative change in florescence (over time) was tracked, and was quantified as a percent relative to a negative sample of Aβ containing only DMSO. If more than 10% inhibition was observed, they were retested at 20μM.

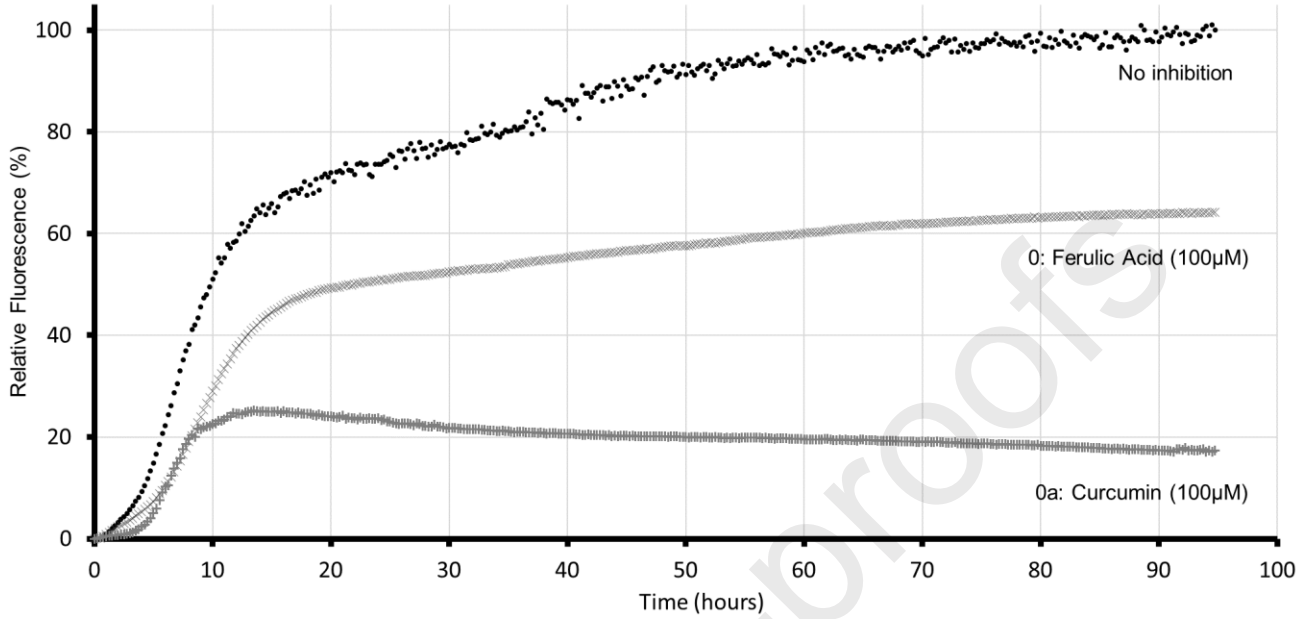

Fig 2. Fibrillization of Aβ, visualized by the fluorescence of thioflavinT (ThT), under inhibition by 100μM of curcumin (+), and ferulic acid (×). No inhibition control (●) was treated with 0.4uL of DMSO to control for the volume of DMSO employed in dissolving compounds.

Table 6
Percent inhibition of Aβ Fibrillization for amide derivatives of ferulic acid

Comp.	Structure	% inh. $A\beta_{40}$ (100μM)	% inh. $A\beta_{40}$ (20μM)	Comp.	Structure	% inh. $A\beta_{40}$ (100μM)	% inh. $A\beta_{40}$ (20μM)
0	Ferulic Acid 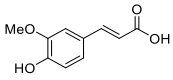	36.83%	9.75%	**0a**	Curcumin 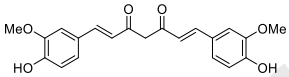	78.15%	65.48%
1	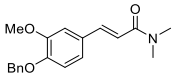	0%		**1f**	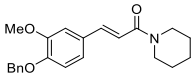	13.42%	7.28%
1a	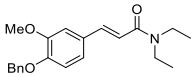	0%		**1fb**	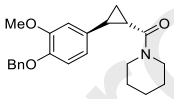	13.26%	0%
1aa	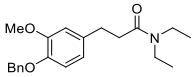	6.49%		**1fc**	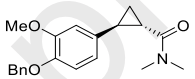	8.81%	
1b	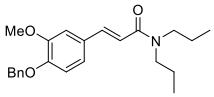	16.96%	9.35%	**1fa**	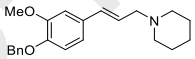	22.31%	0.29%
3e	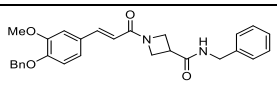	48.23%	14.85%	**3i**	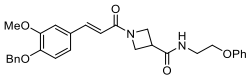	20.57%	5.50%
6	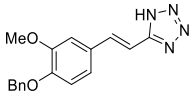	9.56%		**7**	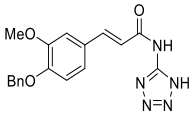	0%	
9	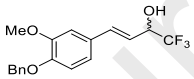	44.11%	0%	**11**	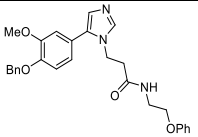	13.82%	5.98%
10	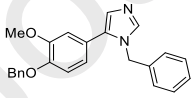	27.53%	2.21%	**12**	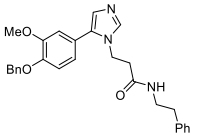	0%	
1ab	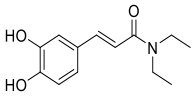	91.88%	73.08%	**11d**	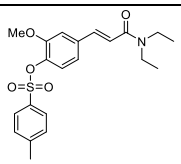	3.62%	1.95%

All compounds were assessed in at least three independent samples, with a minimum of three measurements.

We observed significant discrepancies in fibrillization and oligomerization activities of individual compounds. Derivative **1ab**, for example, strongly inhibits Aβ fibril formation (91.8% at 100μM, 73.1% at 20μM) but only weakly interferes with early oligomerization events (IC_{50} = 119.16μM ± 2.65μM). More broadly, when fibrillization was plotted against oligomerization (inverse IC_{50}), the lack of correlation is clear (Fig. 3). While a weak (R^2 = 0.06) positive trend can be discerned, the majority of compounds effective against one facet of aggregation was ineffective against another. Therefore, compounds which inhibit the assembly of large Aβ fibrils do not necessarily interfere with early nucleation and oligomerization events.

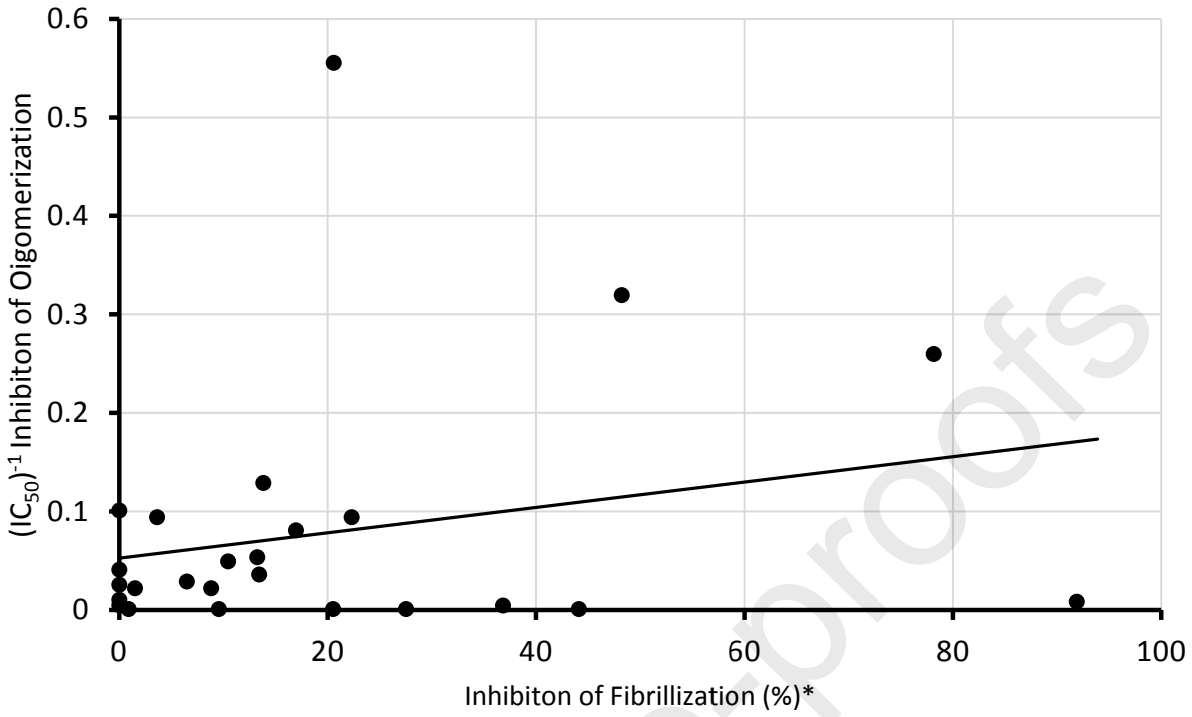

Fig 3. Fibrillization of Aβ, assayed by percent inhibition of thioflavinT (ThT) fluorescence, plotted against inhibition oligomerization (assayed by outlined ELISA protocol).

Likewise, compounds effective against oligomerization, but ineffective against fibrillization were observed (Table 5: compound **1**, **1fa**, **1b**, **1f**, **2i**). Though the precise mechanism of this assembly is unclear, it may arise from the ability of Aβ to form disordered oligomers, which can survive to form less stable, but still viable fibrils. Assays of fibrillization and oligomerization should therefore be treated as distinct measures, and not conflated as a definitive assay of amyloid aggregation. Moreover, optimizing a compound to increase anti-fibrillary activity may be ineffective at preventing oligomerization, and vice-versa. As soluble oligomers, not large fibrils or plaques, are culpable for the neurotoxicity of Aβ, we suggest prioritizing the optimization of anti-oligomeric activity – though ideally both should be considered concurrently.

2.4 Design of Anti-Aβ Aggregates: Lessons from Ferulic Acid Derivatives

The activity of derivatives tested in this investigation suggest that interactions between monomers of Aβ occur over a large surface, ideally targeted by bulky, heavily substituted molecules. However, as a compound grows, solubility, metabolism and BBB penetrance tend to become less favorable. Balancing the dual considerations of increased surface area and optimizing brain bioavailability should therefore be a consideration in future drug development.

In this investigation, the most potent analogs in preventing Aβ oligomerization were **3e** (IC_{50} = 3.13 ± 1.87 μM), **3f** (IC_{50} = 3.65 ± 0.33 μM), **3g** (IC_{50} = 4.78 ± 1.67 μM), **3h** (IC_{50} = 3.61 ± 0.59 μM), and **3i** (IC_{50} = 1.8 ± 0.73 μM). These molecules share an azetidine tether between the ferulic acid and their elongated side chains (derived from β-alanine). They further have multiple π-rich systems on both termini of the molecule, and are sharply bent into a

perpendicular three-dimensional structure. Notably, these molecules are not efficient anti-fibrillary agents, with only modest inhibition of fibrillization at 48.23% and 20.57% for compounds **3e** and **3i** respectively. As such, these compounds may be able to inhibit the neurotoxic oligomerization of Aβ, but may allow for the aggregation into benign plaques to proceed. It is as yet unclear what the impact of this selective inhibition may be on overall disease progression and outcomes, but in light of emerging data on the differing aggregative properties of Aβ, should be a priority for future study.

2.5 Quantitative Structure–Activity Relationship (QSAR) Model

The observations of this investigation were used in the creation of a QSAR model to predict the activity of novel compounds. A total of 79 compounds with measured IC_{50} values were randomly divided into a training set of 54 molecules and a validation set of 25 molecules, each with a varying range of structural features and bio-activities. Using *Molecular Operating Environment* software, 318 descriptors pertaining to various molecular properties were calculated for the training set of molecules. These data proved insufficient to allow for accurate prediction of IC_{50} values; thus a binary prediction model of active vs. inactive was adopted.

The model was developed by sequentially eliminating individual descriptors, based on relative importance, to identify the key factors that would predict compound activity. A binary pIC_{50} ($-\log[IC_{50}]$) threshold of 3.7 was selected to distinguish between the active and inactive compounds. A training set of 36 compounds was created of which 18 were classified as active. The binary QSAR model predicted 34/36 as active (with a cross-validation of 30/36) and 18/18 as inactive (with a cross-validation of 14/18). When the model was applied to the validation set

of 25 molecules, 15 of the 15 active molecules were correctly predicted active, and 7 of the 10 inactive compounds were correctly predicted inactive. The model produced a Cohen's kappa (κ) coefficient of 0.919; and $\kappa = 0.737$ for the validation set – suggesting strong agreement among the predicted and actual results. The descriptors used in the model include the number of carbon atoms present, atomic polarizability, the shape of the molecule, capacity for forming hydrogen bonds, along with the hydrophilic volume of the molecule. Further details of the QSAR model are described in the supplemental information.

3. Conclusion

A diverse library of "curcumin-like" small molecules modelled on amide-derivatives of ferulic acid was constructed to discern the molecular characteristics relevant for the inhibition of Aβ aggregation. Collectively, this library addresses three structural components of ferulic acid: i) the carboxylic acid/amide, ii) the phenyl hydroxyl group, and iii) the rigid, planar backbone between the carboxylic acid and aromatic ring.

Our findings suggest that modifications to these three prominent features have a significant effect on the inhibitory potency. Substitution of the hydroxyl group with a benzyl ether generally increased activity, though subsequent modification of the benzene's electron dynamics lost any gains obtained from the benzene. The amide moiety (formerly the ferulic carboxylic acid) was also crucial for function. Extensive substitutions revealed that the most effective compounds employed a rigid alkyl tether, followed immediately by a second highly polar amide. This regional hydrophobic/hydrophilic transition may provide a specific target for future therapeutics to consider. Extending these molecules with an additional phenyl ring further increased activity, and mimics the extended, terminal-phenyl arrangement of ferulic acid. In general, lengthening the molecule with bulky substitutions increased activity, suggesting a wide amyloidogenic region of interaction between monomers of Aβ; however these may impede the penetrance and solubility of an eventual drug in the brain. As such, balancing the bulk of a molecule to optimize both its interaction with Aβ and its bioavailability will be a critical consideration in future drug design.

Studies should also account for differences in the oligomerization and fibrillization of Aβ. As observed, compounds effective against the oligomerization of Aβ may be ineffective against the

fibrillization of Aβ, and vice-versa. Though compounds effective against both mechanisms of aggregation are the traditional choice, it is conceivable that a compound which inhibits oligomerization, but which allows for the formation of benign fibrils and plaques may both prevent the accumulation of highly toxic soluble oligomers, and allow for the sequestration of Aβ. It is as yet unclear whether this may be a viable therapeutic consideration. This study concluded by employing these data to generate a successful QSAR model capable of making a binary prediction, with high sensitivity and specificity, as to whether a compound was active or not.

With acknowledgement to prior work on ferulic acid and curcumin, we note that the identification of potent anti-Aβ oligomeric agents (compounds **3e-i**) will likely be insufficient for a definitive therapy against AD. Further studies will require more comprehensive analysis within the evolving biochemical paradigm of AD pathology. Moreover, details studies on the degradation and pharmacology of compounds within the human body, including transit of the BBB are necessary. The intention herein was therefore not to identify a novel therapy, but rather to employ a novel library of ferulic acid derivatives to elucidate relevant molecular characteristics to consider in future drug design.

Conflict of interest

The authors declare no conflicts of interest.

Acknowledgements

DFW acknowledged salary support of a Tier 1, Canada Research Chair.

Supplementary data

Supporting information includes supplemental synthesis and design of small molecule derivatives, biological testing procedures and additional details of computational modeling.

Abbreviations

AD, Alzheimer's disease; Aβ, amyloid-β; $A\beta_{42}$, 42 amino acid isoform of β-amyloid; BBB, blood brain barrier; bio-$A\beta_{42}$, biotinylated-$A\beta_{42}$; h, hr; rt, room temperature; ELISA, enzyme-linked immunosorbent assay; ThT, thioflavin T; QSAR, quantitative structure–activity relationship models.

References

1. Perl DP. Neuropathology of Alzheimer's disease. Mt Sinai J Med. 2010;77(1):32-42.
2. Tanzi RE, Bertram L. Twenty years of the Alzheimer's disease amyloid hypothesis: a genetic perspective. Cell. 2005;120(4):545-55.
3. Goedert M, Spillantini MG. A century of Alzheimer's disease. Science. 2006;314(5800):777-81.
4. Mullard A. Alzheimer amyloid hypothesis lives on. Nat Rev Drug Discov. 2016;16(1):3-5.
5. Hamley IW. The amyloid beta peptide: a chemist's perspective. Role in Alzheimer's and fibrillization. Chem Rev. 2012;112(10):5147-92.
6. Luo J, Warmlander SK, Graslund A, Abrahams JP. Cross-interactions between the Alzheimer disease amyloid-beta peptide and other amyloid proteins. S. J Biol Chem. 2017;292(5):2046.

7. Bucciantini M, Giannoni E, Chiti F, Baroni F, Formigli L, Zurdo J, et al. Inherent toxicity of aggregates implies a common mechanism for protein misfolding diseases. Nature. 2002;416(6880):507-11.
8. Glabe CG. Common mechanisms of amyloid oligomer pathogenesis in degenerative disease. Neurobiol Aging. 2006;27(4):570-5.
9. Ono K, Yoshiike Y, Takashima A, Hasegawa K, Naiki H, Yamada M. Potent anti-amyloidogenic and fibril-destabilizing effects of polyphenols *in vitro*: implications for the prevention and therapeutics of Alzheimer's disease. J Neurochem. 2003;87(1):172-81.
10. Hamaguchi T, Ono K, Murase A, Yamada M. Phenolic compounds prevent Alzheimer's pathology through different effects on the amyloid-beta aggregation pathway. Am J Pathol. 2009;175(6):2557-65.
11. Syarifah-Noratiqah S, Naina-Mohamed I, Zulfarina MS, Qodriyah HM. Natural Polyphenols in the Treatment of Alzheimer's Disease. Curr Drug Targets. 2017.
12. Ono K, Hasegawa K, Naiki H, Yamada M. Curcumin has potent anti-amyloidogenic effects for Alzheimer's beta-amyloid fibrils *in vitro*. J Neurosci Res. 2004;75(6):742-50.
13. Yang F, Lim GP, Begum AN, Ubeda OJ, Simmons MR, Ambegaokar SS, et al. Curcumin inhibits formation of amyloid beta oligomers and fibrils, binds plaques, and reduces amyloid *in vivo*. J Biol Chem. 2005;280(7):5892-901.
14. Reinke AA, Gestwicki JE. Structure-activity relationships of amyloid beta-aggregation inhibitors based on curcumin: influence of linker length and flexibility. Chem Biol Drug Des. 2007;70(3):206-15.
15. Kolaj I, Liyanage SI, Weaver DF. Phenylpropanoids and Alzheimer's disease: A potential therapeutic platform. Neurochem Int. 2018;120:99-111.
16. Srinivasan M, Sudheer AR, Menon VP. Ferulic Acid: therapeutic potential through its antioxidant property. J Clin Biochem Nutr. 2007;40(2):92-100.

17. Masuda T, Yamada K, Maekawa T, Takeda Y, Yamaguchi H. Antioxidant mechanism studies on ferulic acid: identification of oxidative coupling products from methyl ferulate and linoleate. J Agric Food Chem. 2006;54(16):6069-74.
18. Kanski J, Aksenova M, Stoyanova A, Butterfield DA. Ferulic acid antioxidant protection against hydroxyl and peroxyl radical oxidation in synaptosomal and neuronal cell culture systems *in vitro*: structure-activity studies. J Nutr Biochem. 2002;13(5):273-81.
19. Sgarbossa A, Giacomazza D, di Carlo M. Ferulic acid: a hope for Alzheimer's disease Therapy from Plants. Nutrients. 2015;7(7):5764-82.
20. Nagai N, Kotani S, Mano Y, Ueno A, Ito Y, Kitaba T, et al. Ferulic acid suppresses amyloid beta production in the human lens epithelial cell stimulated with hydrogen peroxide. Biomed Res Int. 2017;2017:5343010.
21. Mori T, Koyama N, Guillot-Sestier MV, Tan J, Town T. Ferulic acid is a nutraceutical beta-secretase modulator that improves behavioral impairment and alzheimer-like pathology in transgenic mice. PLoS One. 2013;8(2):e55774.
22. Liu YM, Shen JD, Xu LP, Li HB, Li YC, Yi LT. Ferulic acid inhibits neuro-inflammation in mice exposed to chronic unpredictable mild stress. Int Immunopharmacol. 2017;45:128-34.
23. Mori T, Koyama N, Tan J, Segawa T, Maeda M, Town T. Combination therapy with octyl gallate and ferulic acid improves cognition and neurodegeneration in a transgenic mouse model of Alzheimer's disease. J Biol Chem. 2017;292(27):11310-25.
24. Wang H, Sun X, Zhang N, Ji Z, Ma Z, Fu Q, et al. Ferulicacid attenuates diabetes-induced cognitive impairment in rats via regulation of PTP1B and insulin signaling pathway. Physiol Behav. 2017;182:93-100.
25. Sang Z, Pan W, Wang K, Ma Q, Yu L, Yang Y, et al. Design, synthesis and evaluation of novel ferulic acid-O-alkylamine derivatives as potential multifunctional agents for the treatment of Alzheimer's disease. Eur J Med Chem. 2017;130:379-92.

26. Sun Y, Wang B, Ge X, Ding F. Distinct oligomerization and fibrillization dynamics of amyloid core sequences of amyloid-beta and islet amyloid polypeptide. Phys Chem Chem Phys. 2017;19(41):28414-23.
27. Schmit JD, Ghosh K, Dill K. What drives amyloid molecules to assemble into oligomers and fibrils? Biophys J. 2011;100(2):450-8.
28. Necula M, Kayed R, Milton S, Glabe CG. Small molecule inhibitors of aggregation indicate that amyloid beta oligomerization and fibrillization pathways are independent and distinct. J Biol Chem. 2007;282(14):10311-24.
29. Kittner M, Knecht V. Disordered versus fibril-like amyloid beta (25-35) dimers in water: structure and thermodynamics. J Phys Chem B. 2010;114(46):15288-95.
30. LeVine H, 3rd. Biotin-avidin interaction-based screening assay for Alzheimer's beta-peptide oligomer inhibitors. Anal Biochem. 2006;356(2):265-72.

4. Experimental Section

4.1 *In vitro* Biological Evaluation

4.1.1 General Considerations

All chemicals were purchased from Sigma Aldrich (Oakville, ON), aside from DMSO which was purchased from BDH (Mississauga, ON). $A\beta_{40}$ and biotinylated $A\beta_{42}$ were purchased from AnaSpec (Fremont, CA). The streptavidin-HRP conjugate was purchased from Rockland Immunochemicals (Pottstown, PA). All absorbance readings were obtained from the same Biotech Synergy HT plate reader. Water for all assays was obtained on a Milli-Q® Integral Water Purification System.

4.1.2 Measuring Aβ Fibrillization: ThioflavinT Assay

$A\beta_{40}$ was monomerized by dissolution in hexafluoroisopropanol (HFIP) at a concentration of 1 mg/mL. The sample was dried under argon and diluted to a final concentration of 20 μM in 20 mM Tris, 8 μM ThT, 0.3 M NaCl at a pH of 7.4. The solution was then transferred to a black polystyrene 96 well plate, avoiding the outer wells as these tend experience significant evaporation over the 4 days of the experiment. The compounds, dissolved in 100% DMSO at varying concentrations, were added to the 96-well plate, along with DMSO alone (control) in triplicate. ThT fluorescence undergoes a characteristic shift (λ_{ex} =450 nm, λ_{em}=482 nm) as Aβ forms fibrils. Fluorescence was therefore read continuously at 482 nm every 15 minutes for approximately 100 hrs. The control sample provided a 100% aggregation reference, and was used in the calculation of the percent difference (inhibition) of fibrillization. Mean aggregation was determined from the average of three independent samples.

4.1.3 Measuring Aβ Oligomerization: ELISA Assay

Devised by LeVine *et al.*,[30] this assay employs a modified NeutrAvidin (NA)/ Streptavidin (SA) protocol to quantify the relative preponderance of Aβ oligomers to monomers. First, high-binding ELISA plates were coated overnight with NeutrAvidin in 10 mM sodium phosphate buffer, pH 7.5. Biotinylated $A\beta_{42}$ (0.1mg/mL in HFIP) was obtained and dried to a thin film under a stream of argon. It was re-suspended in trifluoroacetic acid (TFA) by vortexing, then dried, washed and dried again with HFIP. Desired compounds were diluted to 2 mM, 1 mM, 500µM, 250µM, 125µM, 62.5µM, and 31µM, in 100% DMSO. A DMSO-only control was incorporated to estimate 100% oligomerization, and a 5% Tween20 negative control was used to estimate 100% inhibition. Compounds and controls were then diluted by 100X in 20mM $NaPO_4$ buffer, containing the monomerized Aβ at a concentration of 10nM. Oligomers were allowed to form for 1 hr, and the reaction was stopped with Tween20. The oligomer preparation was then added to the NA coated plates. After 2 hrs, the plates were washed in TBST. Oligomers were visualized with a standard SA, tetramethylbenzidine (TMB) and peroxide protocol. Mean aggregation and standard deviation were determined from at least three independent samples, with at least three measurements.

4.2 Compound Synthesis

4.2.1 General Considerations

Commercial reagents were purchased from Sigma Aldrich (Oakville, ON), Combi Blocks (San Diego, CA) or Alfa Aesar (Tewksbury, MA) and used without further purification. Reactions were monitored using thin-layer chromatography (TLC) with silica gel on TLC Al foils with a fluorescence indicator of 254 nm. Visualization of the developed plates was performed under UV light (254 nm) or using potassium permanganate (KMnO4),

dinitrophenylhydrazine (DNP), ninhydrin or vanillin stain. Silica gel flash column chromatography was performed on Silicycle 230-400 mesh silica gel or using a CombiFlash® Rf+ equipped with RediSep Rf Disposable Flash columns with 230-400 mesh silica. NMR characterization data were collected at 296 K on a Varian Mercury 400, or a Bruker Avance III spectrometer operating at 300, 400 or 500 MHz for ^{1}H NMR; 75, 101 or 126 MHz for ^{13}C NMR; and 375 and 377 MHz for ^{19}F NMR. ^{1}H NMR and ^{13}C NMR spectra were internally referenced to the residual solvent signal. ^{19}F NMR spectra were internally referenced to TFA (TFA = -76.55 ppm). Data for ^{1}H NMR are reported as follows: chemical shift (δ ppm), multiplicity (s = singlet, d = doublet, t = triplet, q = quartet, m = multiplet, br = broad), coupling constant (Hz), integration. High resolution mass spectra (HRMS) were obtained using Waters ACQUITY UPLC H-Class System (ESI) or a JEOL AccuTOF model JMS-T1000LC mass spectrometer equipped with a Direct Analysis in Real Time (DART) ion source. High performance liquid chromatography (HPLC) was performed on the Waters 2487 Dual λ Absorbance Detector equipped with a C18 reverse phase column. The solvent system used was HPLC grade acetonitrile: water + 0.1 % TFA and compound detection was achieved by monitoring absorbance at 254 nm. Water for the HPLC was obtained on a Milli-Q® Integral Water Purification System.

4.2.2 Select Synthetic Procedures and Compound Characterization

General procedure 1: A dry flask was charged with **S2** (see supporting information, 2.0 mmol), HATU (2.6 mmol) and the contents were dissolved in dry DMF (10 mL, 0.1 M). The solution was stirred for 1 hr at room temperature. TEA (2.8 mmol) was then added, followed by the corresponding amine (2.4 mmol). The reaction was stirred at room temperature for 16-24 hrs,

quenched with H_2O (30 mL) and partitioned in EtOAc (30 mL). The aqueous layer was then extracted with EtOAc (3 × 30 mL), and the combined organic layers were washed with aqueous HCl (2 × 30 mL, 1 M), a saturated aqueous solution of $NaHCO_3$ (2 × 30 mL), water (30 mL) and brine (30 mL); then dried over $MgSO_4$ and concentrated *in vacuo*.

(2E)- 3-[3-Methoxy-4-(phenylmethoxy)phenyl]-N,N-dimethyl-2-propenamide (1) –A flask, charged with compound **S2** (200 mg, 0.7 mmol), was purged with argon for 5 minutes and then suspended in dry DMF (10 mL). EDC·HCl (161 mg, 0.84 mmol) and HOBt (129 mg, 0.84 mmol) were added and the mixture was stirred for 30 minutes at room temperature. Dimethylamine (0.4 mL, 0.77 mmol, 2.0 M in THF) and TEA (0.2 mL, 1.4 mmol) were added and the mixture was stirred under argon. After 16 hrs, the reaction was quenched with H_2O (80 mL) and extracted with EtOAc (3 × 80 mL). The combined organic layers were washed with H_2O (2 × 80 mL), aqueous HCl (80 mL, 1 M), a saturated aqueous solution of $NaHCO_3$ (80 mL), and brine (80 mL). The organic layer was then dried over $MgSO_4$, concentrated *in vacuo* and purified via silica gel column chromatography using an eluent of DCM:MeOH (19:1 v:v) and hexane:EtOAc (2:3 v:v). The purified product was obtained as a white powder (133 mg, 0.42 mmol, 61%). **^{1}H NMR** (300 MHz, $CDCl_3$) δ 7.58 (d, J = 15.3 Hz, 1H), 7.46 – 7.28 (m, 5H), 7.07-7.01 (m, 2H), 6.88-6.82 (m, 1H), 6.72 (d, J = 15.4 Hz, 1H), 5.17 (s, 2H), 3.91 (s, 3H), 3.15 (s, 3H), 3.05 (s, 3H). **HRMS** (ESI, M+H) Calc'd for $C_{19}H_{22}NO_3$ 312.1521, found 312.1598. **Purity by HPLC**: 95.3% (t_R = 11.42 min).

(2E)-N,N-Diethyl-3-[3-methoxy-4-(phenylmethoxy)phenyl]-2-propenamide (1a) – Synthesized according to general procedure 1. The reaction was stirred for 17 hrs on a 2 mmol

scale. The resultant product was purified via silica gel flash column chromatography using hexane:EtOAc (2:3 v:v) as the mobile phase. The pure compound was obtained as a clear oil, which was then lyophilized to yield a white powder as the final product (492 mg, 1.73 mmol, 87%). **^{1}H NMR** (500 MHz, $CDCl_3$) δ 7.63 (d, *J* = 15.3 Hz, 1H), 7.47 – 7.24 (m, 5H), 7.08 – 7.02 (m, 2H), 6.86 (d, *J* = 8.2 Hz, 1H), 6.67 (d, *J* = 15.3 Hz, 1H), 5.18 (s, 2H), 3.92 (s, 3H), 3.54 – 3.37 (m, 4H), 1.25 (t, *J* = 7.0 Hz, 3H), 1.18 (t, *J* = 7.1 Hz, 3H). **^{13}C NMR** (101 MHz, $CDCl_3$) δ 165.97, 149.77, 149.64, 142.30, 136.88, 129.07, 128.72, 128.07, 127.32, 121.35, 115.91, 113.79, 111.11, 71.03, 56.26, 42.37, 41.16, 15.20, 13.38. **HRMS** (ESI, M+H) Calc'd for $C_{21}H_{25}NO_3$ 340.1913, found 340.1932. **Purity by HPLC**: 96.9 % (t_R = 11.8 min).

N,N-Diethyl-3-methoxy-4-(phenylmethoxy)-benzenepropanamide (1aa) – In a Parr apparatus, compound **1a** (24 mg, 0.07 mmol) was dissolved in THF (10 mL) and catalytic Pd/C (2.4 mg, 10 % mmol) was added to the solution. The flask was flushed with nitrogen twice and then flushed with hydrogen. The reaction was pressurized to 20 psi with hydrogen, and shaken for 24 hrs. The Pd/C was removed by vacuum filtration using a celite pad – which was washed with THF. The filtrated was concentrated *in vacuo* to afford the crude product. This was purified via silica gel column chromatography using hexane:EtOAc (1:1 v:v) to obtain the pure product as a pale yellow oil (22 mg, 0.064 mmol, 91%). **^{1}H NMR** (400 MHz, $CDCl_3$) δ 7.21 – 7.01 (m, 5H), 6.58 – 6.53 (m, 2H), 6.44 (dd, *J* = 8.1, 2.1 Hz, 1H), 4.88 (s, 2H), 3.63 (s, 3H), 3.13 (q, *J* = 7.1 Hz, 2H), 2.96 (q, *J* = 7.1 Hz, 2H), 2.68 (t, *J* = 8 Hz, 2H), 2.32 (t, *J* = 8 Hz, 2H), 0.85 (q, *J* = 6.9 Hz, 6H). **HRMS** (ESI, M+H) Calc'd for $C_{21}H_{27}NO_3$ 342.21, found 342.23. **Purity by HPLC**: 98.55% (t_R = 12.02 min).

(E)-3-(3,4-dihydroxyphenyl)-N,N-diethylacrylamide (1ab) – In a flamed dried flask, compound **1a** (0.3 mmol, 102 mg) was dissolved in DCM (3 mL) and the solution was cooled to -78˚C. BBr_3 (1.8 mL, 1.8 mmol, in hexane), was added dropwise at -78˚C. The reaction was warmed to room temperature and stirred for 16 hrs. Once complete, the reaction was quenched with MeOH (14.7 mL) and the solvent was removed *in vacuo* to yield the crude product. The residue was purified via silica gel column chromatography using eluents of hexane:EtOAc (1:4 v:v) and DCM: MeOH (19:1) to yield the pure product as an orange oil which was lyophilized to afford a yellow solid (74.8 mg, 0.297 mmol, 99 %). **^{1}H NMR** (300 MHz, DMSO-d_6) δ 9.37 (s, 2H), 7.31 (d, *J* = 15.1 Hz, 1H), 7.06 (d, *J* = 2.0 Hz, 1H), 6.95 (dd, *J* = 8.2, 2.1 Hz, 1H), 6.79 – 6.71 (m, 2H), 3.35 (q, *J* = 7.1 Hz, 1H), 1.13 (t, *J* = 6.9 Hz, 2H), 1.05 (t, *J* = 7.0 Hz, 2H). **^{13}C NMR** (75 MHz, DMSO) δ 164.93, 147.32, 145.46, 141.67, 126.74, 120.67, 115.63, 114.79, 114.59, 15.27, 13.36. **HRMS** (ESI, M+H) Calc'd for $C_{13}H_{17}NO_3$ 236.1287, found 236.1332. **Purity by HPLC**: 92.5% (t_R = 6.8 min).

(2E)-3-[3-Methoxy-4-[(2-methylphenyl)methoxy]phenyl]-N,N–dipropyl)-2-propenamide (1b/14a) – Synthesized according to general procedure 1, the reaction was run for 16 hrs on a 2 mmol scale, using 1.2 molar equiv of HATU and 1.4 molar equiv of DIPEA. The crude product was purified via silica gel flash column chromatography using hexane:EtOAc (1:1 v:v) as the mobile phase. The pure compound was obtained as a white powder (620 mg, 1.69 mmol, 84%). **^{1}H NMR** (400 MHz, $CDCl_3$) δ 7.62 (d, *J* = 15.2 Hz, 1H), 7.47 – 7.27 (m, 5H), 7.10 – 6.99 (m, 2H), 6.86 (d, *J* = 8.2 Hz, 1H), 6.68 (d, *J* = 15.3 Hz, 1H), 5.18 (s, 2H), 3.92 (s, 3H), 3.39 (t, *J* = 7.5 Hz, 2H), 3.35 (t, *J* = 7.5 Hz, 2H) 1.68 (q, *J* = 7.5, 2H), 1.60 (q, *J* = 7.4 Hz, 2H), 0.95 (t, *J* = 7.4 Hz, 3H), 0.92 (t, *J* = 7.4 Hz, 2H). **^{13}C NMR** (100 MHz, $CDCl_3$) δ 166.39, 149.75, 149.60,

142.16, 136.89, 129.11, 128.73, 128.07, 127.32, 121.21, 116.05, 113.79, 111.16, 71.02, 56.22, 49.99, 48.68, 23.19, 21.29, 11.61, 11.49. **HRMS** (ESI, M+H) Calc'd for $C_{23}H_{30}NO_3$ 368.2226, found 368.2367. **Purity by HPLC:** 100% (t_R = 11.9 min).

(2E)-3-(4-(Benzyloxy)-3-phenylmethoxy)-1-(1-pyrrolidinyl)-2-propen-1-one (1e) – Synthesized according to general procedure 1, the reaction was run for 24 hrs on a 2 mmol scale. The resulting product was purified via silica gel flash column chromatography using hexane:EtOAc (2:3 v:v) as the eluent. The pure compound was obtained as a pale yellow powder (565 mg, 1.7 mmol, 84%). **^{1}H NMR** (400 MHz, DMSO-d_6) δ 7.46 – 7.31 (m, 7H), 7.18 (dd, *J* = 8.4, 2.0 Hz, 1H), 7.04 (d, *J* = 8.4 Hz, 1H), 6.86 (d, *J* = 15.4 Hz, 1H), 5.12 (s, 2H), 3.83 (s, 3H), 3.63 (t, *J* = 6.8 Hz, 2H), 3.39 (t, *J* = 7.2 Hz, 2H), 1.90 (p, *J* = 6.9 Hz, 2H), 1.80 (p, *J* = 6.4 Hz, 2H). **^{13}C NMR** (100 MHz, DMSO-d_6) δ 163.83, 149.24, 149.16, 140.39, 136.89, 128.44, 128.28, 127.91, 127.83, 121.87, 117.76, 113.25, 110.85, 69.83, 55.74, 46.07, 45.63, 25.63, 23.90. **HRMS** (ESI, M+H) Calc'd for $C_{21}H_{24}NO_3$ 338.1756, found 338.1895. **Purity by HPLC**: 94.7% (t_R = 11.1 min).

(2E)-3-[3-methoxy-4-(phenylmethoxy)phenyl]-1-(1-piperidinyl)-2-propen-1-one (1f) – A flame dried flask, charged with compound **S2** (568 mg, 2 mmol), EDCI (537 mg, 2.8 mmol) and HOBt (378 mg, 2.8 mmol), was purged with argon for 10 minutes before the addition of dry DMF (10 mL). The mixture was stirred at room temperature for 1 hr, then TEA (0.39 mL, 2.4 mmol) was added. Piperidine (0.24 mL, 2.4 mmol) was added dropwise to the resulting yellow solution. The mixture was then stirred at room temperature for 24 hrs. Once complete, the reaction was quenched with H_2O (50 mL) and partitioned in EtOAc (50 mL). The layers were

separated, and the aqueous layer was extracted with EtOAc (3 × 40 mL). The combined organic layers were washed with aqueous HCl (2 × 20 mL, 1 M), saturated aqueous solution of $NaHCO_3$ (2 × 20 mL), brine (2 × 20 mL), dried over $MgSO_4$ and concentrated *in vacuo* to afford the crude product. This was purified via silica gel flash column chromatography using hexane:EtOAc (4:1 v:v + 1% AcOH) as the mobile phase. The final product was obtained as a white powder (645 mg, 1.83 mmol, 92%). **^{1}H NMR** (400 MHz, DMSO-d_6) δ 7.49 – 7.26 (m, 7H), 7.17 (dd, *J* = 8.4, 2.0 Hz, 1H), 7.13 (d, *J* = 15.3 Hz, 1H), 7.03 (d, *J* = 8.3 Hz, 1H), 5.11 (s, 2H), 3.83 (s, 3H), 3.65 (br, 2H), 3.53 (br, 2H), 1.60 (td, *J* = 6.5, 3.7 Hz, 2H), 1.49 (s, 4H). **^{13}C NMR** (100 MHz, DMSO-d_6) δ 164.53, 149.25, 149.10, 141.48, 136.91, 128.43, 127.90, 127.84, 122.05, 116.10, 113.17, 110.66, 69.82, 55.79, 38.25, 24.24. **HRMS** (ESI, M+H) Calc'd for $C_{22}H_{22}NO_4$ 352.1913, found 352.1940. **Purity by HPLC**: 92.5% (t_R = 11.4 min).

(2-(4-(Benzyloxy)-3-methoxyphenyl)cyclopropyl)(piperidin-1-yl)methanone (1fb) – A flame dried two-neck flask, purged with argon for 10 minutes, was charged with trimethylsulfoxonium iodide (550 mg, 2.5 mmol) and suspended in dry DMSO (4 mL). Sodium hydride (100 mg, 2.5 mmol, 60% in mineral oil) was added portion-wise and the mixture was stirred for 20 minutes. In a separate flask, compound **1f** (351 mg, 1 mmol) was suspended in dry DMSO (5 mL) and was added dropwise to the mixture. The reaction was stirred at room temperature for 30 minutes, then heated to 80˚C. After 22 hrs, the reaction was cooled to room temperature and quenched with aqueous HCl (5 mL, 2M), diluted with brine (20 mL) and extracted with EtOAc (3 × 30 mL). The combined organic layers were washed with brine (2 × 30 mL), dried over $MgSO_4$ and concentrated *in vacuo*. There resulting product was purified via silica gel column chromatography using an eluent of hexane:EtOAc (6:4 v:v) to yield the pure product as an

orange oil which was lyophilized to a yellow solid (125 mg, 0.34 mmol, 34%). The *trans* diastereomer was produced, of which enantiomers were present. **^{1}H NMR** (400 MHz, $CDCl_3$) δ 7.51 – 7.25 (m, 5H), 6.82 (d, *J* = 8.3 Hz, 1H), 6.75 (d, *J* = 2.1 Hz, 1H), 6.59 (dd, *J* = 8.3, 2.1 Hz, 1H), 5.15 (s, 2H), 3.91 (s, 3H), 3.60 (dp, *J* = 11.1, 5.6 Hz, 4H), 2.45 (ddd, *J* = 9.0, 6.2, 4.2 Hz, 1H), 1.93 (ddd, *J* = 8.3, 5.4, 4.2 Hz, 1H), 1.68 (qd, *J* = 5.7, 3.5 Hz, 2H), 1.65 – 1.54 (m, 5H), 1.23 (ddd, *J* = 8.3, 6.2, 4.3 Hz, 1H). **^{13}C NMR** (100 MHz, CDCl3) δ 170.26, 149.69, 146.77, 137.34, 134.46, 128.59, 127.86, 127.31, 117.71, 114.35, 110.90, 71.27, 56.12, 46.78, 43.44, 26.74, 25.61, 25.00, 24.76, 23.11, 15.57. **HRMS** (ESI, M+H) Calc'd for $C_{23}H_{28}NO_3$ 366.2069, found 366.2125. **Purity by HPLC**: 96.6% (t_R = 9.66 min).

2-(4-(Benzyloxy)-3-methoxyphenyl)-N,N-dimethylcyclopropane-1-carboxamide (1fc) – A flamed dried two-neck flask, purged with argon for 10 minutes, was charged with trimethylsulfoxonium iodide (121 mg, 0.55 mmol) and suspended in dry DMSO (1.6 mL). Sodium hydride (22 mg, 0.55 mmol, 60% in mineral oil) was added portion-wise and the mixture was stirred for 20 minutes. In a separate flask, compound **1** (50 mg, 0.16 mmol) was suspended in dry DMSO (1.1 mL) and was added dropwise to the mixture. The reaction was stirred at room temperature for 30 minutes and then heated to 80˚C. After 16 hrs, the reaction was allowed to cool to room temperature and quenched with aqueous HCl (3 mL, 2M). The product was diluted with brine (10 mL) and extracted with EtOAc (3 × 15 mL). The combined organic layers were washed with brine (2 × 15 mL), dried over $MgSO_4$ and concentrated *in vacuo*. The resulting crude product was purified via silica gel column chromatography using an eluent of DCM:MeOH (19:1 v:v) to yield the pure product as a white powder (24 mg, 0.073 mmol, 45%). The reaction produced the *trans* diastereomer, of which both enantiomers were collected. **^{1}H**

NMR (400 MHz, $CDCl_3$) δ 7.33 – 7.11 (m, 5H), 6.65 (d, *J* = 8.2 Hz, 1H), 6.58 (d, *J* = 2.1 Hz, 1H), 6.43 (dd, *J* = 8.4, 2.1 Hz, 1H), 4.98 (s, 2H), 3.74 (s, 3H), 2.99 (s, 3H), 2.85 (s, 3H), 2.30 (ddd, *J* = 9.0, 6.3, 4.2 Hz, 1H), 1.77 (ddd, *J* = 8.3, 5.3, 4.2 Hz, 1H), 1.43 (ddd, *J* = 9.0, 5.3, 4.2 Hz, 1H), 1.08 (ddd, *J* = 8.3, 6.3, 4.2 Hz, 1H). **HRMS** (ESI, M+H) Calc'd for $C_{20}H_{24}NO_3$ 326.1678, found 326.1700. **Purity by HPLC**: 94.6% (t_R = 14.7 min).

General procedure 2: Compound **S5** or **S5a** (0.26 mmol) and HATU (0.31 mmol) were dissolved in anhydrous DMF (2.6 mL, 0.1 M), and stirred for 30 minutes before DIPEA (0.52 mmol) followed by the corresponding amine (0.31 mmol, 1.2 equiv) were added. The reaction was heated to 35˚C then stirred at room temperature until the reaction was shown to be complete by TLC (usually within 16-24 hrs). The reaction was then quenched with brine (15 mL) and diluted with EtOAc (15 mL). The aqueous layer was extracted with EtOAc (3 × 10 mL) and the combined layers were washed with aqueous HCl (2 × 10mL, 1M), an aqueous solution of saturated $NaHCO_3$ (2 × 10 mL), brine (2 × 10 mL) and dried over $MgSO_4$, and concentrated *in vacuo* to yield the crude product.

(S,E)-3-(4-(benzyloxy)-3-methoxyphenyl)-1-(2-(piperidine-1-carbonyl)pyrrolidin-1-yl)prop-2-en-1-one (2a) – The product was synthesized according to general procedure 2 using compound **S5** as the starting carboxylic acid. The crude product was purified via silica gel flash column chromatography using hexane:EtOAc (1:9 v:v) as the mobile phase and the pure product was isolated as a pale orange powder (98 mg, 0.22 mmol, 84%). NMR showed a mixture of rotamers A and B in approximately a 10:1 ratio. **^{1}H NMR** (300 MHz, $CDCl_3$) δ 7.67 – 7.52 (m, 1H, A+B), 7.46 – 7.27 (m, 5H, A+B), 7.12 – 6.92 (m, 2H, A+B), 6.84 (d, *J* = 8.1 Hz, 1H, A+B),

6.62 and 6.24 (d, *J* = 15.4 Hz, 1H, A+B), 5.17 (s, 2H), 5.02 and 4.82 (dd, *J* = 8.0, 3.9 Hz, 1H, A+B), 4.01 – 3.28 (m, 9H), 2.28 – 1.73 (m, 5H), 1.71 – 1.41 (m, 5H). **HRMS** (ESI, M+H) Calc'd for $C_{27}H_{33}N_2O_4$ 449.2240, found 449.2421. **Purity by HPLC**: 99.8% (t_R = 8.96 min).

(S,E)-N-Benzyl-1-(3-(4-(benzyloxy)-3-methoxyphenyl)acryloyl)pyrrolidine-2-carboxamide (2b) – The product was synthesized according to general procedure 2 using compound **S5** as the carboxylic acid. The crude product was purified via silica gel flash column chromatography using hexane:EtOAc (1:7 v:v) as the mobile phase and the pure product was obtained as a pale yellow powder (119 mg, 0.25 mmol, 97%). NMR showed a mixture of rotamers A and B in approximately a 5:1 ratio. **^{1}H NMR** (300 MHz, $CDCl_3$) δ 7.61 (d, *J* = 15.3 Hz, 2H, A+B), 7.44 – 7.23 (m, 9H, A+B), 7.14 – 6.80 (m, 4H, A+B), 6.55 and 6.33 (d, *J* = 15.4 Hz, 1H, A+B), 5.17 – 5.15 (m, 2H, A+B), 4.78 – 4.71 and 4.58 – 4.53 (m, 1H, A+B), 4.51 – 4.44 (m, 1H, A+B), 4.36 – 4.27 (m, 1H, A+B), 3.88 and 3.84 (s, 3H, A+B), (s, 1H), 3.81 – 3.53 (m, 2H), 2.57 – 1.71 (m, 4H). **HRMS** (ESI, M+H) Calc'd for $C_{29}H_{31}N_2O_4$ 471.2284, found 471.2251. **Purity by HPLC**: 98.4% (t_R = 9.06 min).

General procedure 3: A flame dried flask was purged with argon for 5 minutes and charged with compound **S8** (0.5 mmol), HATU (0.65 mmol) and dry DMF (5 mL, 0.1 M). The reaction mixture was stirred at room temperature for 1 hr. DIPEA (1.5 mmol, 3 equiv) was added to the mixture followed by the corresponding amine (0.65 mmol). The mixture was heated to 50˚C and stirred for 16-24 hrs. The reaction was cooled to room temperature, diluted with brine (50 mL), and extracted with EtOAc (3 × 30 mL). The combined organic layers were washed with aqueous

HCl (50 mL, 1 M), a saturated aqueous solution of $NaHCO_3$ (50 mL) and brine (50 mL), then dried using $MgSO_4$ and concentrated *in vacuo*.

(E)-1-(3-(4-(benzyloxy)-3-methoxyphenyl)acryloyl)-N,N-diethylazetidine-3-carboxamide (3a) – Synthesized according to general procedure 3 (for 24 hrs, at a 0.24 mmol scale); the crude product was purified using silica gel flash column chromatography using hexane:EtOAc (1:19 v:v) as the eluent. The pure product was dried under reduced pressure to yield a white solid (64.3 mg, 0.144 mmol, 66%). **^{1}H NMR** (300 MHz, $CDCl_3$) δ 7.49 (d, *J* = 15.5 Hz, 1H), 7.40 – 7.22 (m, 5H), 6.98 – 6.95 (m, 2H), 6.78 (d, *J* = 8.8 Hz, 1H), 6.24 (d, *J* = 15.6 Hz, 1H), 5.11 (s, 2H), 4.63 (t, *J* = 7.1 Hz, 1H), 4.25 (td, *J* = 9.5, 8.9, 4.4 Hz, 2H), 4.12 – 4.06 (m, 1H), 3.85 (s, 3H), 3.50 (tt, *J* = 9.0, 6.2 Hz, 1H), 3.42 – 3.24 (m, 2H), 3.12 (qd, *J* = 7.1, 2.1 Hz, 2H), 1.11 (t, *J* = 6.8 Hz, 3H), 1.06 (t, *J* = 6.8 Hz, 3H). **HRMS** (ESI, M+H) Calc'd for $C_{25}H_{31}N_2O_4$ 447.1920, found 447.1942. **Purity by HPLC**: 92.1% (t_R = 8.76 min).

(*E*)-3-(4-(benzyloxy)-3-methoxyphenyl)-1-(3-(3,3-difluoroazetidine-1-carbonyl)azetidin-1-yl)prop-2-en-1-one (3b) – Synthesized according to general procedure 3; the reaction was run for 24 hours on a 0.218 mmol scale with: 1.3 molar equiv of amine, 2 molar equiv of HATU, and 3 molar equiv of DIPEA. The crude product was purified via silica gel flash column chromatography using DCM:MeOH (19:1 v:v) as the mobile phase to yield the pure product as a white solid (36.1 mg, 0.081 mmol, 37%). **^{1}H NMR** (300 MHz, $CDCl_3$) δ 7.28 (d, *J* = 15.6 Hz, 1H), 7.17 – 6.96 (m, 5H), 6.79 – 6.72 (m, 2H), 6.57 (d, *J* = 8.8 Hz, 1H), 5.99 (d, *J* = 15.6 Hz, 1H), 4.89 (s, 2H), 4.34 – 4.23 (m, 1H), 4.18 – 3.83 (m, 7H), 3.63 (s, 3H), 3.09 (tt, *J* = 8.8, 6.1 Hz, 1H). **^{13}C NMR** (75 MHz, $CDCl_3$) δ 171.11, 166.56, 150.00, 149.74, 142.05, 136.71, 128.72,

128.20, 128.10, 127.30, 121.98, 114.86, 113.57, 113.05, 110.72, 70.93, 56.17, 51.77, 50.42, 29.75. **^{19}F NMR** (377 MHz, $CDCl_3$, TFA standard) δ -101.35 (p, *J* = 10.5 Hz). **HRMS** (ESI, M+H) Calc'd for $C_{24}H_{25}F_2N_2O_4$ 443.1782, found 443.1813. **Purity by HPLC**: 96.7% (t_R = 10.03 min).

General procedure 4: A dry flask was charged with compound **S10** (0.28 mmol,), HATU (0.34 mmol) and anhydrous DMF (2.8 mL, 0.1 M). This solution was stirred for 1 hr and DIPEA (0.56 mmol), followed by the corresponding amine (0.34 mmol) were added to the solution. The reaction was initially heated to 35˚C and stirred at room temperature until the reaction was shown to be complete by TLC, (typically within 16-24 hrs). The reaction was quenched with brine (15 mL) and diluted with EtOAc (15 mL). The aqueous layer was extracted with EtOAc (3 × 10 mL) and the combined layers were washed with aqueous HCl (2 × 10 mL, 1M), an aqueous solution of saturated $NaHCO_3$ (2 × 10 mL), brine (2 × 10 mL) and dried over $MgSO_4$, then concentrated *in vacuo* to yield the crude product.

(E)-3-(4-(Benzyloxy)-3-methoxyphenyl)-N-(3-oxo-3-(piperidin-1-yl)propyl)acrylamide (4) – Synthesized according to general procedure 4; the crude product was purified via silica gel flash column chromatography using hexane:EtOAc (1:9 v:v) as the mobile phase and the pure product was isolated as a pale yellow powder (111 mg, 0.26 mmol, 94%). **^{1}H NMR** (300 MHz, $CDCl_3$) δ 7.50 (d, *J* = 15.6 Hz, 1H), 7.45 – 7.28 (m, 5H), 7.04 – 6.94 (m, 2H), 6.84 (d, *J* = 8.3 Hz, 1H), 6.64 (t, *J* = 6.3 Hz, 1H), 6.25 (d, *J* = 15.6 Hz, 1H), 5.17 (s, 2H), 3.91 (s, 3H), 3.67 (q, *J* = 5.8 Hz, 2H), 3.55 (t, *J* = 5.5 Hz, 2H), 3.35 (t, *J* = 5.4 Hz, 2H), 2.56 (t, *J* = 5.4 Hz, 2H), 1.66 – 1.69 (m, 2H), 1.59 – 1.47 (m, 4H). **^{13}C NMR** (MHz, $CDCl_3$) δ 170.11, 166.06, 149.75, 149.68,

140.52, 136.82, 128.73, 128.38, 128.08, 127.32, 121.94, 119.21, 113.53, 109.97, 70.95, 56.07, 46.47, 42.74, 35.27, 33.00, 26.40, 25.66, 24.54. **HRMS** (ESI, M+H) Calc'd for $C_{25}H_{31}N_2O_4$ 423.2284, found 423.2282. **Purity by HPLC**: 100 % (t_R = 8.82 min).

(*E*)-*N*-(3-(Benzylamino)-3-oxopropyl)-3-(4-(benzyloxy)-3-methoxyphenyl)acrylamide (5a) – Synthesized according to general procedure 3; the crude product was purified via silica gel flash column chromatography using hexane:EtOAc (1:9 v:v) as the mobile phase. The pure product was isolated as a white powder (116 mg, 0.26 mmol, 93%). **^{1}H NMR** (300 MHz, $CDCl_3$) δ 7.42 (d, *J* = 15.6 Hz, 1H), 7.37 – 7.18 (m, 9H), 7.17 – 7.12 (m, 1H), 6.98 – 6.87 (m, 2H), 6.77 (d, *J* = 8.2 Hz, 1H), 6.45 (t, *J* = 6.1 Hz, 1H), 6.16 (d, *J* = 15.6 Hz, 1H), 6.00 (t, *J* = 5.1 Hz, 2H), 5.10 (s, 2H), 4.36 (d, *J* = 5.7 Hz, 2H), 3.83 (s, 3H), 3.59 (q, *J* = 6.0 Hz, 2H), 2.43 (t, *J* = 5.8 Hz, 2H). **HRMS** (ESI, M+H) Calc'd for $C_{28}H_{31}N_2O_5$ 445.2127, found 445.2113. **Purity by HPLC**: 97.1% (t_R = 8.65 min).

The synthesis and characterization of all intermediaries and all other compounds are described in the included supporting information.

Declaration of interests

☒ The authors declare that they have no known competing financial interests or personal relationships that could have appeared to influence the work reported in this paper.

☐The authors declare the following financial interests/personal relationships which may be considered as potential competing interests: